TU Delft

Delft University of Technology

Document Version
Final published version

Licence
Dutch Copyright Act (Article 25fa)

Citation (APA)
Guo, P., Chang, Z. Y., Pertijs, M. A. P., & Costa, T. L. (2025). A Single-Inductor-Based High-Voltage Transmit Beamformer for Wearable Ultrasound Devices Achieving 88% fCV2Power Reduction. In *2025 IEEE International Solid-State Circuits Conference, ISSCC 2025* IEEE. https://doi.org/10.1109/ISSCC49661.2025.10904513

Important note
To cite this publication, please use the final published version (if applicable).
Please check the document version above.

Copyright
In case the licence states “Dutch Copyright Act (Article 25fa)”, this publication was made available Green Open Access via the TU Delft Institutional Repository pursuant to Dutch Copyright Act (Article 25fa, the Taverne amendment). This provision does not affect copyright ownership.
Unless copyright is transferred by contract or statute, it remains with the copyright holder.

Sharing and reuse
Other than for strictly personal use, it is not permitted to download, forward or distribute the text or part of it, without the consent of the author(s) and/or copyright holder(s), unless the work is under an open content license such as Creative Commons.

Takedown policy
Please contact us and provide details if you believe this document breaches copyrights.
We will remove access to the work immediately and investigate your claim.

This work is downloaded from Delft University of Technology.

35.1 A Single-Inductor-Based High-Voltage Transmit Beamformer for Wearable Ultrasound Devices Achieving 88% fCV² Power Reduction

Peng Guo, Zu-Yao Chang, Michiel A. P. Pertijs, Tiago L. Costa

Delft University of Technology, Delft, The Netherlands

Compared to its implant-based electrical counterpart, ultrasonic vagus nerve stimulation alters neuronal activity through mechanical ultrasound waves, emerging as a promising non-invasive therapy for managing drug-resistant epilepsy [1]. To enable immediate intervention following seizure detection, a low-power, compact wearable device is sought to send continuous low- or medium-intensity focused ultrasound waves to targeted areas, such as the cervical vagus nerve (Fig. 35.1.1). The integration of transducer arrays and ASICs supporting high-voltage (HV) pulsing enables on-chip electrical transmit (TX) beamforming with sufficient acoustic pressure at the focal spot and allows for the miniaturization of such devices, but it also poses challenges in power consumption. A conventional class-D pulser (Fig. 35.1.1) exhibits excessive fCV^2 power loss due to the charging and discharging of the transducer's capacitance. A resonant pulser, in contrast, uses an inductor to recycle the associated energy, ideally reducing fCV^2 loss to 0. However, previous works [2,3] would require multiple off-chip inductors to implement TX beamforming, making them unsuitable for our application. Moreover, the use of body-diode conduction for energy recycling significantly reduces power efficiency [2]. This paper presents a resonant TX beamformer architecture that employs a single inductor to pulse groups of transducer elements at different phases, thus enabling the required efficient continuous-wave TX beamforming.

To reduce hardware overhead, continuous-wave TX beamforming often employs a Fresnel delay profile (Fig. 35.1.1) combined with phase delay quantization, i.e., wrapping the quantized phase delay between 0 and 2π [4]. A 32-element transducer array is divided into 8 phase delay groups ($PD_{1\text{-}8}$) based on the distance of the elements to the desired focal spot, each corresponding to one of 8 quantized phase delays (Fig. 35.1.2). To generate the rising and falling transitions, the inductor (L_0) is cyclically connected to the phase delay groups and their antiphase group (e.g., $PD_{1,5}$, $PD_{2,6}$, etc.) when the inductor current drops to zero (Φ_{L1-8}). Between the transitions, the transducers are connected to ground or to the supply (Φ_{S1-8}), both to replenish the energy lost during the resonating period and to provide the energy for ultrasound transmission. To prevent overvoltage, a non-uniform quantization scheme is employed so that each group contains an equal number of elements and thus a roughly identical capacitance (Fig. 35.1.3). Compared to the 8-phase uniform quantization in [4], which would result in unequal group sizes, this scheme only slightly degrades the focal spot pressure, making it well-suited for our application. This architecture allows energy to resonate between the transducers' capacitance and the inductor, eliminating the need for body-diode conduction and thus improving both power efficiency and immunity to latch-up.

A clock frequency of 8× the transducer center frequency (f_0) is employed. The durations of the transitions (Φ_{L1-8}) need to be precisely tuned to achieve zero-current switching, thereby maximizing power efficiency and compensating for PVT variations. This is accomplished via a PWM-based resonating time control loop, incorporating a fully differential slope-based zero-current detector (ZCD) followed by eight 6b up/down counters and a DLL-based PWM generator (Fig. 35.1.3). To detect the slope of the differential voltage (ΔV_{L0}) across the inductor, the slope-based ZCD employs a pair of capacitors ($C_{DP/N}$), which are connected to ground via switches ($S_{P/N}$) during each rising/falling period (e.g., Φ_{L1}). After this period, the switches are turned off for a short interval (τ), during which a voltage (ΔV_{CP}) proportional to the slope of the differential voltage across the inductor (ΔV_{L0}) is built at the input of a comparator, followed by a polarity decision. The decision results, corresponding to 8 rising and falling durations, are cyclically fed to 8 dedicated up/down counters, allowing for separate tuning of each duration. The outputs of these 8 counters are concatenated and input to an edge combiner, which accordingly selects two edges out of 128 phases generated from a DLL and combines them into a PWM signal (PWM_{SYS}) in a center-aligned fashion, i.e., the center of the PWM signal is always aligned with the falling edge of the clock signal (CK_{SYS}). This scheme aims to align all rising/falling transitions approximately at their mid-transition points (Fig. 35.1.2), thus reducing delay errors resulting from PVT variations. The PWM signal and clock signal are XOR-encoded into a single signal (CKPWM), similar to Manchester encoding, and then distributed across the entire chip via a global distribution network before being decoded locally (e.g., PWM_{CHn}, CK_{CHn}), thereby minimizing skew and phase delay errors between different pulser channels. This feedback loop continuously adjusts the resonating period towards its optimized value (Fig. 35.1.3), which can be further read out and preloaded as the initial value of the counters, facilitating quick loop settling.

Back-to-back isolating high-voltage (HV) switches are used to switch the inductor among the 32 transducer elements (Fig. 35.1.3). As these switches experience steep voltage changes due to the rapid switching across a wide voltage range, a robust bootstrap gate driver is implemented to ensure safe operation (Fig. 35.1.4), employing a bootstrap capacitor (C_{BST}) to generate a floating supply of approximately 5V, a latch-based level shifter, and a modified C-element [5]. C_{BST} provides the charge to turn on the back-to-back switches, while being replenished to 5V via M_{RP} when the transducer is discharged to ground. The floating supplies (V_{BST}, V_{MID}) can vary rapidly, while the latch cannot immediately charge and discharge two level-shifting capacitors ($C_{LSP/N}$) in response, causing the latch outputs to bear either both low or both high states. In contrast with a conventional SR latch [6], the modified C-element retains its output during these states, thereby ensuring reliable switching.

The ASIC is fabricated in a 180nm BCD process, incorporating 32 pulser channels and the feedback control (Fig. 35.1.7). Figure 35.1.4 shows measured steady-state outputs of the ASIC, equipped with a 1.1μH off-chip inductor, operating at 2MHz and a 36V HV supply. All pulser channels are loaded with 120pF capacitors. The deviation from the ideal phase delays is <0.012 rads, thanks to the center-aligned PWM scheme and XOR encoding. To characterize the feedback loop, the voltages of the inductor and the output of a pulser were measured (Fig. 35.1.5), with the resonating duration initially set to 25.6ns. The loop, enabled at 11μs, adjusted the duration to 52ns within approximately 9μs. The measured HV power consumption is 1.23W at 36V, with all 32 channels loaded with 120pF capacitors, demonstrating an 88.2% reduction in fCV^2 losses compared to class-D mode (Fig. 35.1.5). The low-voltage domain of the ASIC, supplied by 1.8V and 5V, consumes 7mW and 75mW, respectively, which is negligible compared to the HV power consumption.

Additionally, the chip was used to drive a 32-element 1-D CMUT transducer array at 2 MHz, featuring a 315μm pitch and a 120pF element capacitance. The measured power consumption shows a 70.4% reduction at 36V compared to class-D mode, further validating the effectiveness of our design (Fig. 35.1.5). For acoustic characterization (Fig. 35.1.6), a water tank was mounted on the CMUT array. The chip was programmed to steer the ultrasound beam to various focal spots. Ultrasound pressure was measured using a hydrophone positioned by an XYZ stage. The resulting pressure maps clearly show the focal spots at their configured locations (Fig. 35.1.6). A comparison with prior art aiming at reducing fCV^2 loss (Fig. 35.1.7) shows that this work achieves the highest TX voltage and a substantial improvement in efficiency, all while enabling beamforming with a single inductor, making it a promising solution for low-power wearable ultrasound stimulation devices.

Acknowledgement:
This work is part of the RELIEVE project (No. 101099481) funded by the European Innovation Council. The authors would like to thank the Philips MEMS Foundry for providing the CMUT samples.

2025 IEEE International Solid-State Circuits Conference (ISSCC) | 979-8-3315-4101-9/25/$31.00 ©2025 IEEE | DOI: 10.1109/ISSCC49661.2025.10904513

Authorized licensed use limited to: TU Delft Library. Downloaded on July 28,2026 at 12:18:09 UTC from IEEE Xplore. Restrictions apply.

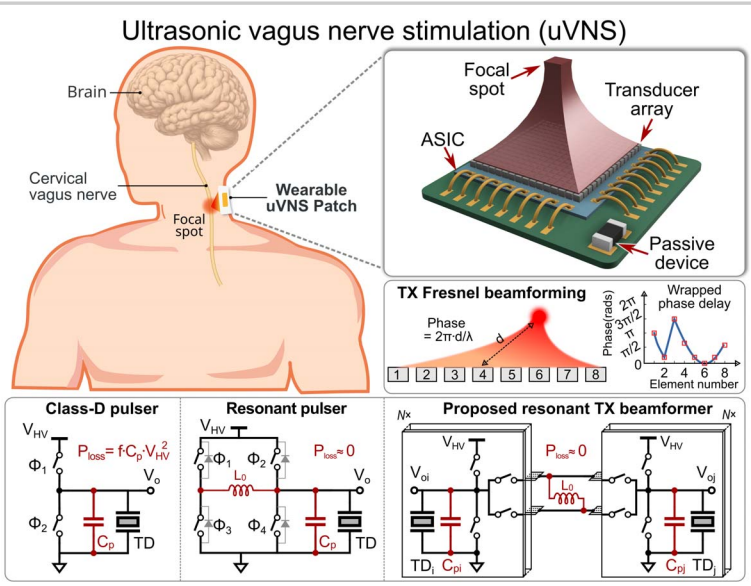


Figure 35.1.1: System overview of a wearable uVNS patch and comparison between class-D, resonant pulser, and the proposed TX beamformer.

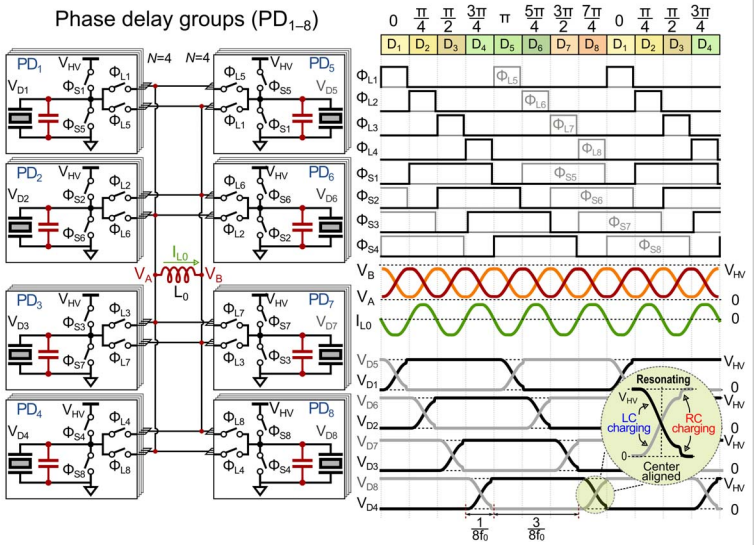


Figure 35.1.2: System architecture of the single-inductor-based TX beamformer and its timing diagram, with inset showing details of a resonating period.

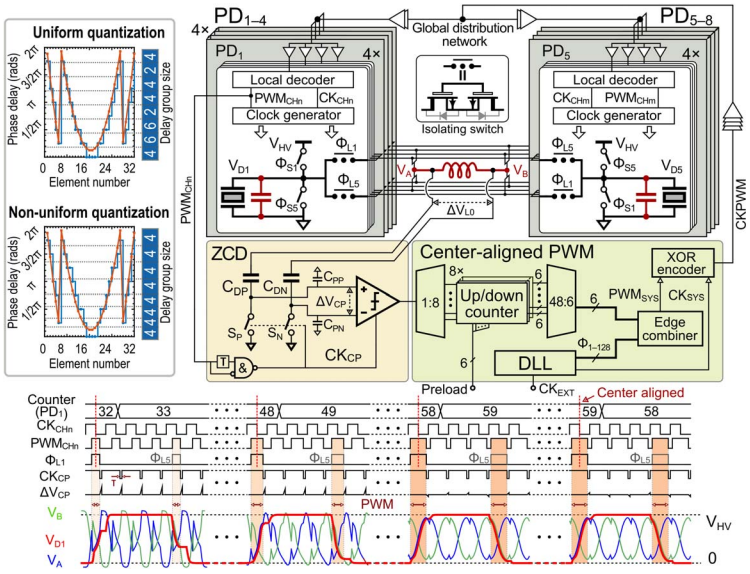


Figure 35.1.3: Phase delay quantization for a 32-element transducer array, the PWM-based resonating time control and its timing details.

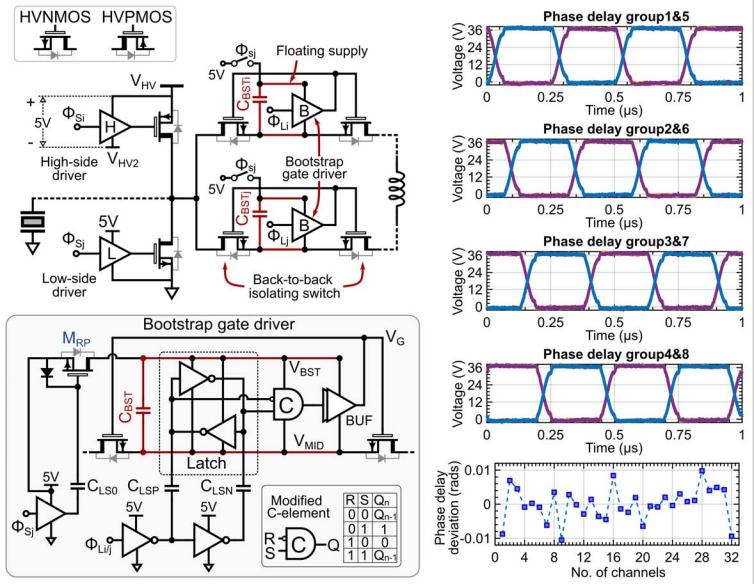


Figure 35.1.4: Circuit diagram of the pulser, measured 32-channel output waveforms and the extracted deviation from the ideal phase delays.

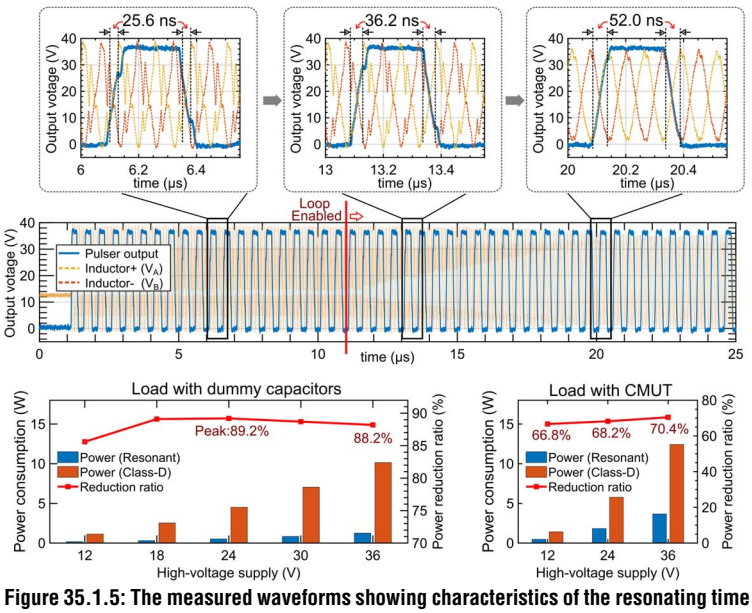


Figure 35.1.5: The measured waveforms showing characteristics of the resonating time control loop and the power consumptions for different loads.

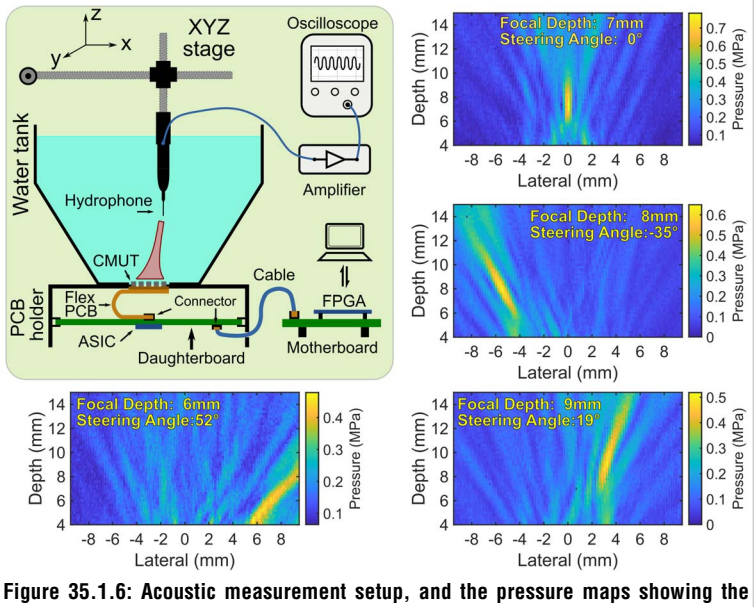
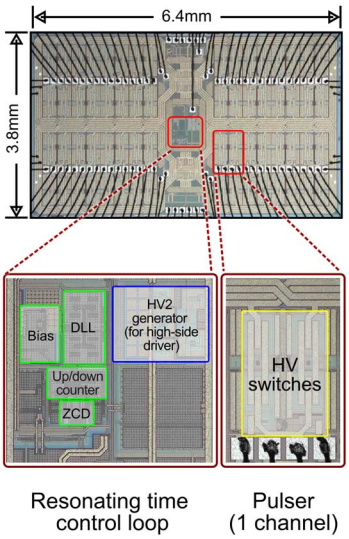


Figure 35.1.6: Acoustic measurement setup, and the pressure maps showing the focused beam profiles at various focal spots.

Authorized licensed use limited to: TU Delft Library. Downloaded on July 28,2026 at 12:18:09 UTC from IEEE Xplore. Restrictions apply.



Comparison with state-of-the-art TX circuits for ultrasound applications

	This work	ISSCC [7]	JSSC [8]	JSSC [9]	ESSCIRC [10]	ISSCC [2]	ISSCC [3]
Process	180n BCD	65n	180n HV	180n	180n BCD	180n BCD	180n BCD
Transducer	CMUT	PMUT	CMUT	PMUT	PMUT	PZT	CMUT
Channel	32	16	4	36	4	1	1
Load cap	120 pF	2.5 pF	40 pF	15.4 pF	235 pF	820 pF	120 pF
TX beam-forming	Yes	Yes	No	No	No	No	No
TX voltage	36V	4.8V	30V	13.2V	32V	30V	30V
Operating frequency	2M	7.8M	3.3M	5M	250k	1M	2.5M
fCV^2 power reduction	88.2%	69%	38%	42.2%	80%	73.1%	63%

Figure 35.1.7: Micrograph of the ASIC and comparison with state-of-the-art TX designs.

References:

[1] H. F. J. Gonzalez, et al., "Vagus Nerve Stimulation for the Treatment of Epilepsy," *Neurosurg. Clin. N. Am.*, vol. 30, no. 2, pp. 219-230, Apr. 2019.

[2] J. Choi, et al., "An Energy-Replenishing Ultrasound Pulser with 0.25CV^2f Dynamic Power Consumption," *ISSCC*, pp. 486-487, Feb. 2021.

[3] I. Bellouki, et al., "A Resonant High-Voltage Pulser for Battery-Powered Ultrasound Devices," *ISSCC*, pp. 106-107, Feb. 2024.

[4] H. Rivandi and T. L. Costa, "A 2D Ultrasound Phased-Array Transmitter ASIC for High-Frequency US Stimulation and Powering," *IEEE TBioCAS*, vol. 17, no. 4, pp. 701-712, Aug. 2023.

[5] I. E. Sutherland, "Micropipelines," *Commun. ACM*, vol. 32, no. 6, pp. 720-738, June 1989.

[6] Y. M. Hopf, et al., "A Compact Integrated High-Voltage Pulser Insensitive to Supply Transients for 3-D Miniature Ultrasound Probes," *IEEE SSCL*, vol. 5, pp. 166-169, 2022.

[7] M. Gourdouparis, et al., "An Ultrasound-Powering TX with a Global Charge-Redistribution Adiabatic Drive Achieving 69% Power Reduction and 53° Maximum Beam Steering Angle for Implantable Applications," *ISSCC*, pp. 102-103, Feb. 2024.

[8] K. Chen, et al., "Ultrasonic Imaging Transceiver Design for CMUT: A Three-Level 30-Vpp Pulse-Shaping Pulser With Improved Efficiency and a Noise-Optimized Receiver," *IEEE JSSC*, vol. 48, no. 11, pp. 2734-2745, Nov. 2013.

[9] J. Lee, K.-R. Lee, B. E. Eovino, et al., "A 36-Channel Auto-Calibrated Front-End ASIC for a pMUT-Based Miniaturized 3-D Ultrasound System," *IEEE JSSC*, vol. 56, no. 6, pp. 1910-1923, Jun. 2021.

[10] J. Pelgrims, K. Myny, and W. Dehaene, "A 36V Ultrasonic Driver for Haptic Feedback Using Advanced Charge Recycling Achieving 0.20CV^2f Power Consumption," *ESSCIRC*, pp. 159-162, Sep. 2021.

Authorized licensed use limited to: TU Delft Library. Downloaded on July 28,2026 at 12:18:09 UTC from IEEE Xplore. Restrictions apply.

979-8-3315-4101-9/25/$31.00 ©2025 IEEE